Acta Biomaterialia 122 (2021) 236–248

Contents lists available at ScienceDirect

Acta Biomaterialia

journal homepage: www.elsevier.com/locate/actbio

Full length article

A matter of size? Material, structural and mechanical strategies for size adaptation in the elytra of *Cetoniinae* beetles

Meisam Asgari[a,1], Nicolas A. Alderete[a,1], Zhaowen Lin[a,1], Ryan Benavides[c], Horacio D. Espinosa[a,b,*]

[a] Theoretical and Applied Mechanics Program, Northwestern University, Evanston, IL 60208, USA
[b] Department of Mechanical Engineering, Northwestern University, Evanston, IL 60208, USA
[c] Department of Mechanical Engineering, University of Texas at Austin, Austin, TX 78712, USA

ARTICLE INFO

Article history:
Received 18 August 2020
Revised 15 December 2020
Accepted 17 December 2020
Available online 21 December 2020

Keywords:
Beetles
Elytra
Biomaterials
Biodiversity
Scaling
Bioinspiration
In situ experiments

ABSTRACT

Nature's masterfully synthesized biological materials take on greater relevance when viewed through the perspective of evolutionary abundance. The fact that beetles (order *Coleoptera*) account for a quarter of all extant lifeforms on Earth, makes them prime exponents of evolutionary success. In fact, their forewings are acknowledged as key traits to their radiative-adaptive success, which makes the beetle elytra a model structure for next-generation bioinspired synthetic materials. In this work, the multiscale morphological and mechanical characteristics of a variety of beetle species from the *Cetoniinae* subfamily are investigated with the aim of unraveling the underlying principles behind Nature's adaptation of the elytral *bauplan* to differences in body weight spanning three orders of magnitude. Commensurate with the integral implications of size variation in organisms, a combined material, morphological, and mechanical characterization framework, across spatial scales, was pursued. The investigation revealed the simultaneous presence of size-invariant strategies (chemical compositions, layered-fibrous architectures, graded motifs) as well as size-dependent features (scaling of elytral layers and characteristic dimensions of building blocks), synergistically combined to achieve similar levels of biomechanical functionality (stiffness, energy absorption, strength, deformation and toughening mechanisms) in response to developmental and selection constraints. The integral approach here presented seeks to shed light on Nature's solution to the problem of size variation, which underpins the diversity of beetles and the living world.

Statement of significance

The ability of Nature to adapt common structural motifs and leverage a limited pool of materials to respond to evolutionary pressures is unparalleled. Beetles, in particular, embody the finest expressions of Nature's deftness, as evinced by their pervasiveness and the richness of their diversity. Here, material, structural and mechanical characteristics of the elytra of four different species of *Cetoniinae* beetles are compared to elucidate the natural strategies guiding adaptations to body size. Commensurate with the integral implications of body size on functionality, a variety of multimodal and multiscale characterization methods are used, revealing the presence of size-invariant and size-dependent features. As such, this work seeks to establish a roadmap for future systematic, comparative analyses of beetle biomechanics, scaling and phylogenetics.

1. Introduction

Coleoptera, the distinct order of insects comprised by beetles, embodies the quintessential evolutionary success, totaling more than 350,000 identified species (i.e., 25% of all animal lifeforms) interspersed across most regions of the globe, and displaying a myriad of remarkable features that have enthralled humans since the days of Ancient Egypt. The diversity and success of the Coleoptera order are demonstrated by the sheer numbers of their taxonomic classification, which to date establishes four Suborders, each one further subdivided into Series, Superfamilies, Families, and Species (*Polyphaga*: 5 Series, 16 Superfamilies, 144 Families, 350,000 Species; *Adephaga*: 10 Families, 40,000 Species, *Archeostomata*: 5 Families, 50 Species and *Myxophaga*: 1 Series, 2

* Corresponding author.
E-mail address: espinosa@northwestern.edu (H.D. Espinosa).
[1] These authors contributed equally to this work

https://doi.org/10.1016/j.actbio.2020.12.039
1742-7061/

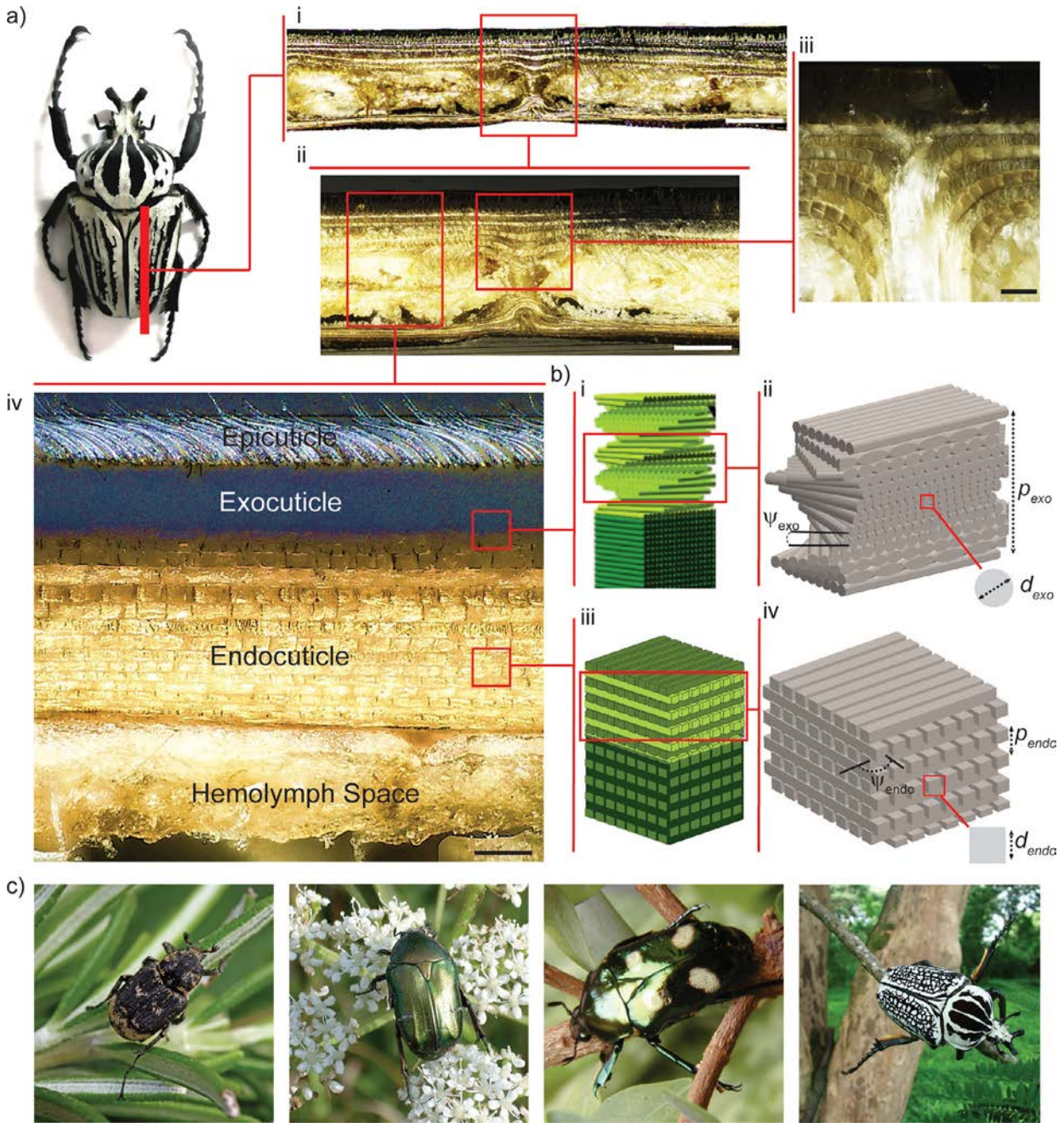

Fig. 1. a) Confocal laser microscopy images of longitudinal cross section of the elytra of Goliathus orientalis (i-ii, Scale: 100 μm), with detailed views of the trabeculae (iii, Scale: 20 μm), and dorsal cuticle with major layers identified (iv, Scale: 30 μm). b) Helicoidal and pseudo-orthogonal arrangement of chitin micro- and macrofibers in the exocuticle (i-ii) and endocuticle (iii-iv), respectively. c) Male adult Cetoniinae beetles, from left to right: Valgus hemipterus (Courtesy of ©entomart), Cetonia aurata pisana (Courtesy of F. Vitali, CC-BY-NC), Jumnos ruckeri (Courtesy of T. Vrána) and Goliathus orientalis (Courtesy of P. Malec). All figures in c) were obtained with written permission from owners.

Superfamilies, 4 Families, 65 Species) [1,2]. Though a matter of debate [3], the remarkable radiative-adaptive success of beetles is generally ascribed to the rise of angiosperms (i.e., *Angiospermae*, flowering plants) ca. 140 Mya. [4] and to the evolution of modified, hardened forewings exclusive to beetles, the Elytra, which facilitated access to novel ecological niches under new environmental pressures [5]. The remarkableness of beetle elytra rests primarily on its multifunctional character, involving chemical, physical and mechanical characteristics that give rise to a plethora of adaptations that facilitate predatory protection, thermal insulation [6], hydration and nourishment [7], locomotion [8] and reproduction [9].

From a material and mechanical perspective, the elytra exemplify Nature's unparalleled ability to design natural composite structures from a limited pool of constituents with excellent functional mechanical properties (e.g., high stiffness and toughness, low weight). The elytra exhibit a layered structure conventionally separated into four major regions (Fig. 1a, i-iv): Epicuticle, Exocuticle, Endocuticle and Hemolymph Space (HS). The latter separates the dorsal and ventral cuticles, a by-product of the epithelial folding of the larval thorax during development, which are bridged by columns of connective tissue known as trabeculae [10]. The outermost layer, the epicuticle, is typically 1-2 μm thick, carries lesser mechanical value and is primarily associated to sensorial functions.

The exocuticle exhibits a fibrillar mesh of chitin crystallites and protein (diameter d_{exo}) arranged in a helicoidal fashion (i.e., Bouligand structure, Fig. 1b, i-ii) with variable pitch (p_{exo}, length for a rotation of π), pitch angles (ψ_{exo}, twist angle between successive plies within one helicoid), which confers the structure with piercing resistance and toughness [10,11]. Next, the endocuticle exhibits a plywood-like structure where parallel chitinous macrofibrils, of diameter d_{endo}, are stacked following a characteristic pitch (p_{endo}, length for a rotation of π) to form thicker layers or plies (Fig. 1b, iii-iv) rotated with respect to successive layers by an angle ψ_{endo} [11], responsible for the overall elytral stiffness. While the broad repertoire of elytral adaptations and the exquisite multiscale material architecture elicit the idea of evolutionary design, insight into the way these structures vary from one species to another, and how the generic *bauplan* (i.e., the generalized structural body plan) is fine-tuned to cope with the particulars of each species, remains scarce.

In an attempt to address this gap, we investigated the elytra of four species of beetles belonging to the same taxonomical subfamily (*Cetoniinae*, ca. 40,000 species), but primarily differentiated by macroscopic size, with the objective of shedding light on the elytral adaptations to changes in body size and its implications on the overall mechanical performance of these structures. In particular, male adult specimens from the species *Valgus hemipterus* (Linnaeus, 1758), *Cetonia aurata pisana* (Linnaeus, 1761), *Jumnos ruckeri* (Saunders, 1839) and *Goliathus orientalis* (Moser, 1909) were selected on the basis of their genetic similarity and their markedly distinct adult body sizes (Fig. 1c), which encompass three orders of magnitude in body weight. *Cetoniinae* beetles, or flower chafers due to their preference for plants, tree sap and fruits, are proficient diurnal flyers and distributed worldwide with *Cetonia aurata pisana* and *Valgus hemipterus* primarily in the Palearctic and Nearctic ecozones, *Jumnos ruckeri* in the Indomalaya ecozone, and *Goliathus orientalis* localized in the Afrotropic savannah. Aiming at establishing comparative relationships between species, we first describe the characterization of macro-, micro- and nanostructural morphologies and compositions of their elytra, via a combination of multiscale microscopy and spectroscopy techniques. Next, we outline the measurement of the anisotropic elastic properties of chitin nanofibers, via atomic force microscopy indentation, and analyze and compare the overall mechanical performance of the elytra, by means of *in situ* SEM beam bending testing. By integrating the identified morphological and fiber properties, using composite beam theory, we examine the role of size and body weight on the elytra flexural stiffness, failure stress, energy dissipation, and failure mechanics. We close with a discussion of the elytral bauplan size-invariant and size-variant strategies and the utility of the introduced multiscale methodology in future systematic and comprehensive comparative studies of beetle biomechanics, scaling, and phylogenetics.

2. Materials and methods

2.1. Beetle collection and sample preparation

Male, adult specimens of *Valgus hemipterus, Cetonia aurata pisana, Jumnos ruckeri* and *Goliathus orientalis* beetles were purchased air-dried from BioQuip Inc. (Compton, CA). Upon arrival, samples were inspected for characteristic features (e.g., body shape, coloration features), and subsequent macroscopic and microscopic measurements of body and elytral sizes were contrasted to existing literature for additional validation. Removed elytra were placed in silicon molds in EMbed-812 resin (Electron Microscopy Science, Hatfield, PA), and polymerized at $65^{\circ}C$ for 48 hours. Subsequently, longitudinal sections from the embedded samples were cut using a diamond blade on a Tech Cut 5 saw with dicing accessory (Allied High Tech Products Inc., Rancho Dominguez, CA). For characterization studies (SEM-EDS, AFM), samples were mounted on SEM stubs and thin slices of 50 *nm* thickness cut using an Ultracut-S ultramicrotome (Leica Biosystems Nussloch GmbH) with a diamond knife (DiATOME, Hartfield, PA) to ensure a surface roughness below 5 *nm*. In the case of AFM nanoindentation, the sample thickness was maintained above3 *mm*, to avoid substrate effects. For bending tests, whole elytra samples were first attached from one longitudinal side to a substrate using hydrosoluble adherent wax. Longitudinal rectangular beams were then excised from the other side of the samples using a low-concentration, diamond metal bond wafering blade on the Tech Cut 5 saw with dicing accessory. All samples used were in dehydrated state.

2.2. Confocal laser scanning microscopy (CLSM) and atomic force microscopy (AFM)

An Olympus LEXT OLS5000 laser confocal scanning microscope (Olympus Corporation, Japan) was used to image the elytral sections. AFM imaging and mechanical tests were conducted using a Park Systems XE-120 AFM (Park Systems, Santa Clara, CA). Biotool high resolution qp-BioAC/Quartz cantilevers with a 2 nm defined conical tip (60 μ m length, 0.1 N/m spring constant, 50 kHz nominal resonance frequency; Nanotools USA LLC, Henderson, NV), and super-sharp standard Force Modulation Mode Reflex Coating cantilevers with diamond-like carbon nanotip of radius $2-3nm$ ($2.8\ N/m$ spring constant, 75 *kHz* nominal resonance frequency; Nanotools USA LLC, Henderson, NV) were used for imaging. For indentation measurements, Non-Contact High Resonance cantilevers with integrated spherical tip of radius 50 *nm* (40 N/m spring constant, Nanotools USA LLC, Henderson, NV) were used. Indentation rates of 0.1 $\mu m/s$ were used with maximum indentation depths of 30 *nm*. All AFM measurements were performed in ambient temperature ($20-25^{\circ}C$). Prior to each indentation test, the precise spring constant of the cantilever was calibrated with the thermal noise fluctuations in air [12,13].

AFM characterization of the helicoidal structure and anisotropic properties of nanofibers in the exocuticle followed the original methodology presented by Espinosa and co-workers [14]. One beetle per species was imaged and indented. Three nanoindentations per point were made, and ten points per pitch were examined. The inherent viscoelasticity of biological materials was not considered in the present work and their incorporation is left for future work.

2.3. Scanning electron microscopy (SEM) and macro- microstructural features measurements

SEM imaging of longitudinal cross sections was performed using a FEI Nova NanoSEM 600 (FEI Co., Hillsboro, OR, USA) to measure the thickness of the elytra and the elytral sublayers, and verify the structural features obtained via CLSM and AFM. Excised sections were adhered on aluminum stubs using double-sided conductive carbon tape, and coated with a 6 *nm* thick Osmium layer.

Elytra and elytral sublayers thicknesses were measured in two different beetles for each species, each one measured in at least 10 segments. The thicknesses of each layer were later averaged to reduce them to a single point, representative to the species, for the power-law relationships derived.

2.4. Energy dispersive spectroscopy (EDS) and Fourier transform spectroscopy (FTIR)

EDS maps were acquired during $10-15$ *min* using an Oxford Aztec X-max 80 SDD detector within a cold source field-emission Hitachi SU8030 SEM operated at 20 *kV* accelerator voltage (Hi-

tachi Ltd., Japan). EDS characterization was done on one beetle per species.

Attenuated total reflection Fourier Transform Spectroscopy was performed on uncoated polished cross sections of Goliathus Orientalis using a Bruker Lumos FTIR Microscope (Bruker Corporation, Billerica, MA, USA). Peak identification was performed using MATLAB R2016b (MathWorks, Natick, MA, USA).

2.5. In situ SEM three-point bending test

The behavior of elytra in the small deformations regime under three-point bending was tested using a commercial Alemnis nanomechanical testing platform (Alemnis GmbH). Rectangular beams of 10 *mm* in length (L), 2 *mm* in width and thickness (t, dictated by elytral thickness) were cut according to the ASTM D790 standard and glued to a 3D printed fixture. Tests were performed under displacement control, achieved by the piezoelectric (PZT) actuators within the loading head, at a nominal speed of 0.1 $\mu m/s$ with a wedge-shaped diamond punch. A displacement sensor located on the loading head measured the resulting enforced displacement (1 *nm* Root Mean Square, RMS, noise at 200 *Hz*), and a load sensor underneath the sample holder was employed to measure the load (4 μN RMS noise at 200 *Hz*). The applied strains were determined after correction for thermal drift and machine compliance. The tests were conducted inside an FEI Nova NanoSEM 600 (FEI Co., Hillsboro, OR, USA).

The large deformation regime up to failure was studied using a micro-mechanical testing platform (Ernest F. Fullam, Inc., Latham, NY), allowing for greater displacement. The tests were displacement-controlled at constant quasi-static loading rates, and during each test, the loading sequence was paused at the onset of signatures in the force-displacement measurements. Such signatures were interpreted as indicative of significant microstructural changes in the samples. In each pause, the beams were examined in high magnification mode to identify, monitor, and track damage initiation and propagation. All tests were video recorded (*Supplementary Videos 1-3*). The larger-size nature of *Goliathus orientalis* samples entailed obvious advantages from a visualization and feature-identification perspective. For this reason, and due to the fact that the majority of mechanisms observed in *Goliathus orientalis* were also observed in the other species, *Goliathus orientalis* is discussed in detail. Conversely, difficulties stemming from the intrinsic small size of *Valgus Hemipterus* made it impossible to explore its response both in the small and large deformations regime. Two samples for each beetle species were tested (one in the small deformation regime and one in the large deformation regime).

2.6. Statistical analysis

Ordinary Least Squares regressions were used to fit the arithmetic mean body weight and arithmetic mean thicknesses of the elytral layers correlation. Two-sided standard deviation errors bars are used to illustrate variability in body mass and layer thickness in each data point. Arithmetic means and standard deviations were used to characterize pitch length, fiber diameter and elastic constants from AFM imaging and nanoindentation measurements, as well as bending stiffnesses. The statistical distributions of fiber diameters for all species were fitted from histograms with a bin size of 20 and a beta distribution.

3. Results

3.1. Macro- and micro-morphological features

The taxonomical proximity of the selected beetles, enforced by design in this study, entails a set of shared morphological traits, but also allows for sharp differences in bulk morphology and appearance, where macroscopic size constitutes the most prominent one from a biomechanical point of view. On the commonality side, these species typically exhibit stout and flattened bodies, distinctive lamellate (fan shaped, lobed) antennae with their insertion visible from above, exposed pygidium (i.e., dorsal tergite of last external abdominal segment), unforked and equally sized tarsal claws, and no horns, with the exception of *Goliathus orientalis* [15]. Among the macroscopic distinctions, *Goliath* beetles are characteristically patterned with sharply contrasting black and white stripes, while *Valgus* beetles merely show black or dark brown scales. Interestingly, unlike the aforementioned species, both *Cetonia aurata pisana* and *Jumnos ruckeri* beetles exhibit structural coloration, evidenced by their distinctive spotted metallic green color, indicative of dedicated microstructural photonic features within the epicuticle.

Most strikingly, these beetles encompass a wide range of body sizes and weights, that can reach up to one and three orders of magnitude differences, respectively, from the smallest to the largest species (Fig. 2a,b). Macroscopically, body sizes and weights follow similar trends as the respective elytral sizes and weights (Fig. 2b), which underscores the central role these hard exoskeletons play in the survival of these insects and supports the use of body weight as a representative measure of size. Leveraging on the concept of evolutionary allometry (biological scaling), which explores size-scaling relationships across species, the elytral thicknesses and the thicknesses of the exocuticle and endocuticle were measured and related to the body weight (W) of each beetle species. Interestingly, when the aforementioned variables across the four beetle species are compared, they reveal underlying power law relationships of the type $y \propto W^k$, where y stands for a structural dimension of relevance. These type of allometric laws are common in size-scaling approaches to biomechanical features, as it is well known that isometric scaling ($k = 1$) of support elements (e.g., bones) leads to untenable structures prone to structural failure (e.g., collapse, buckling, etc.) [16]. Our results appear to suggest negative allometric scaling for all variables ($k < 1$), meaning faster growth of the allometric organ as compared to weight. In particular, elytral thickness and exocuticle thickness present similar allometric scaling exponents (k=0.30, R^2=0.82 and k=0.25, R^2=0.91, respectively), both higher than the corresponding exponent found for the endocuticle (k=0.14, R^2=0.85).

3.2. Microstructural features and hierarchical functional gradients

Topographic imaging of the elytra of the four beetle species, via ultra-fine atomic force microscopy, reveals the existence of repeating patterns indicative of the periodic Bouligand structure and the following, alternating Plywood-like arrangement of fiber bundles or macro-fibers (Fig. 3a,b). The Bouligand structure is detected by the characteristic striated texture (Fig. 3b), highlighting the successive completions of helicoidal pitches along the thickness. High-resolution imaging also evidences the presence of dimensional gradients in the pitch size (p_{exo}) of the helicoidal composite, with the pitch increasing in the exocuticle to endocuticle transition region (Fig. 3b). Conversely, the endocuticles of the four beetles present a characteristic pseudo-orthogonal or cross-ply arrangement, as evidenced by the alternating texture (Fig. 3a). The endocuticles are comprised of macro-fibers, which are bundles of tightly packed microfibrils with a primarily unidirectional alignment. The presence of thin gaps between these bundles, akin to a brick and mortar structure, furthermore reveals that these endocuticles exhibit the characteristic *balken* morphology, from the German term for beams, as opposed to the continuum ply morphology (Fig. 3c, ii-v).

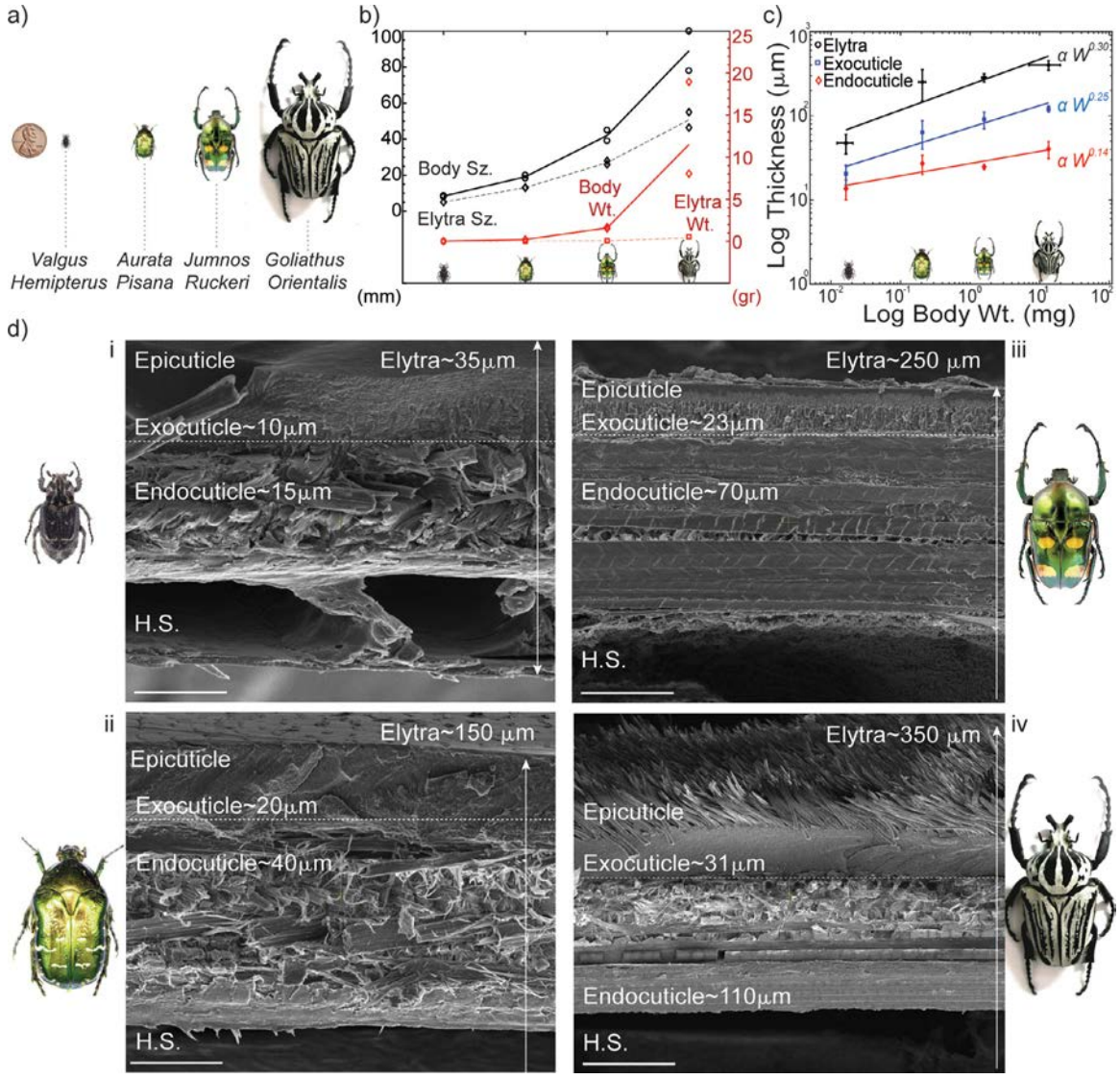

Fig. 2. a) Size comparison of the Valgus hemipterus, Cetonia aurata pisana, Jumnos ruckeri and Goliathus orientalis (coin for scale). b) Body and elytral sizes and weights for each species. c) Evolutionary allometric relationships between elytral thickness and exo- endocuticle thicknesses. d) SEM images of elytral longitudinal sections of Valgus hemipterus (i), Cetonia aurata pisana (ii), Jumnos ruckeri (iii) and Goliathus orientalis (iv). Scale: 10, 20, 30, 50 μm.

Table 1
Exocuticle structural metrics for *Valgus hemipterus, Cetonia aurata pisana, Jumnos ruckeri* and *Goliathus orientalis*.

Beetle Species	Pitch Length (p_{exo}) (nm)	Fiber Diameter (d_{exo}) (nm)	Layers per Pitch (n_{exo})	Twisting Angle (ψ_{exo}) (deg)
Valgus hemipterus	114.6 ± 0.01	20.1 ± 11.8	6	30
Cetonia aurata pisana	207.5 ± 3.3	37.2 ± 22.8	6	30
Jumnos ruckeri	387.9 ± 9.9	44.4 ± 26.1	8	20
Goliathus orientalis	693.5 ± 18.4	55.6 ± 25.6	12	14

Beyond the common structural architectures and dimensionally-graded motifs found in all the species, detailed analysis of nanoscale features within their exocuticles uncovers differences concerning the intricate Bouligand arrangement and the nanofibers which comprise it. Based on the finest features revealed by AFM contact mode imaging, and following the methodology presented in a previous work [14], the pitch length (p_{exo}) and fiber diameter (d_{exo}) distribution are determined for each species, revealing increasing values for increasing beetle sizes, suggesting a size-dependent strategy (Table 1, Fig. 4). Across species, the average pitch size (p_{exo}) was found to lie in the range of $115 - 694$ nm whereas the average diameter (d_{exo}) of individual fibers was found to lie within the range of $20 - 56$ nm. Using the average pitch lengths and fiber diameters measured, the number of layers comprising each exocuticle pitch (*i.e.*, $n_{exo} = p_{exo}/d_{exo}$), and the relative twisting angle between successive layers (*i.e.*, $\psi_{exo} = \pi / n_{exo}$) are estimated (Table 1). These results reveal helicoidal geometries commensurate with body size (i.e., greater size, greater pitches), further emphasizing the adaptation of identical building blocks (microfibers) to changes in size. Reduction of twisting angles translates into a more helicoidal pattern in the material architecture, which yields greater in-plane isotropy as well as stiffness to inelastic deformation. Furthermore, a reduction in twisting angle entails a reduced mismatch between successive layers and promotes lesser interlaminar stresses. Interestingly, the statistical distribution of fiber diameters

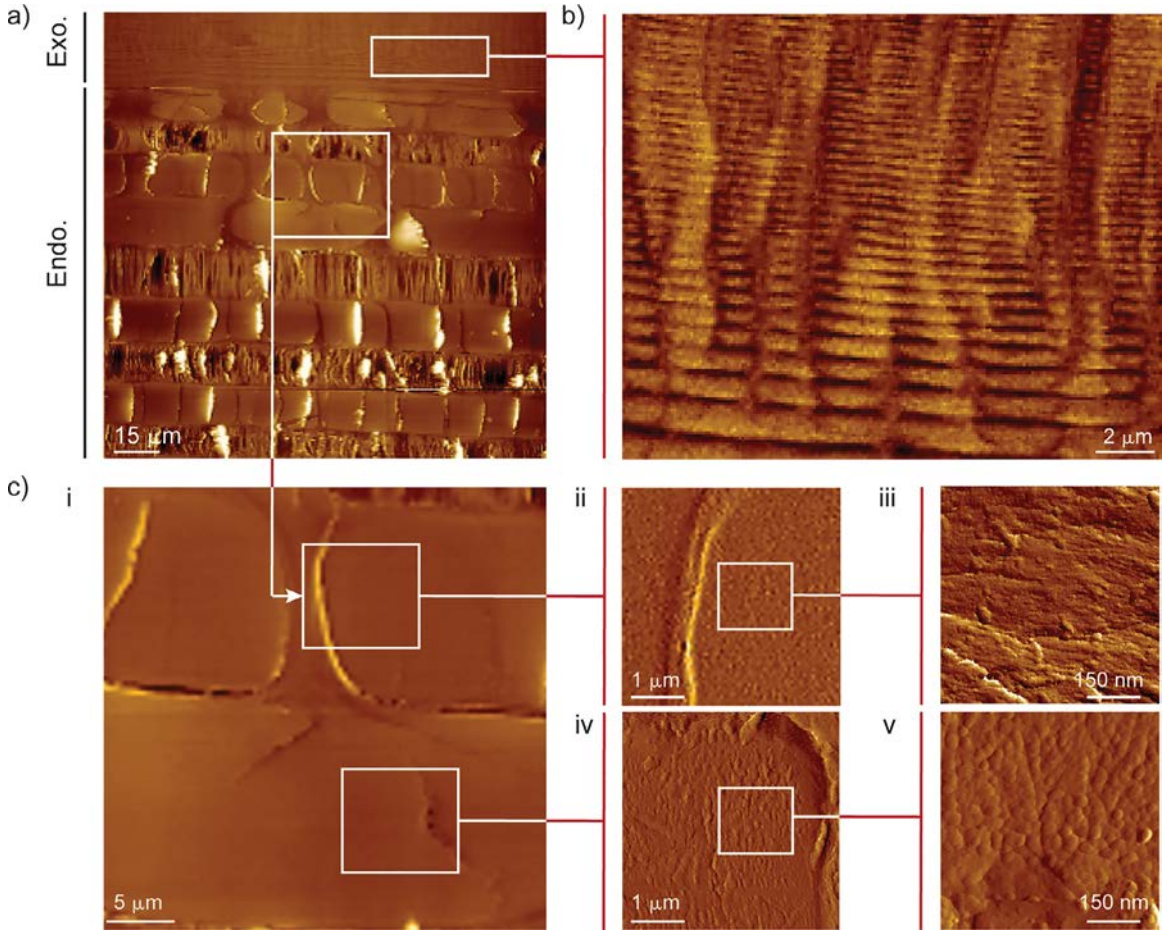

Fig. 3. AFM images of Goliathus orientalis procuticle. a) Exo- and Endocuticle, b) Detailed view of exocuticle with dimensional graded motif towards the endocuticle interface, c) Detailed views of endocuticle encompassing two adjacent orthogonal layers (i), 0° ply (ii-iii) and 90° ply (iv-v).

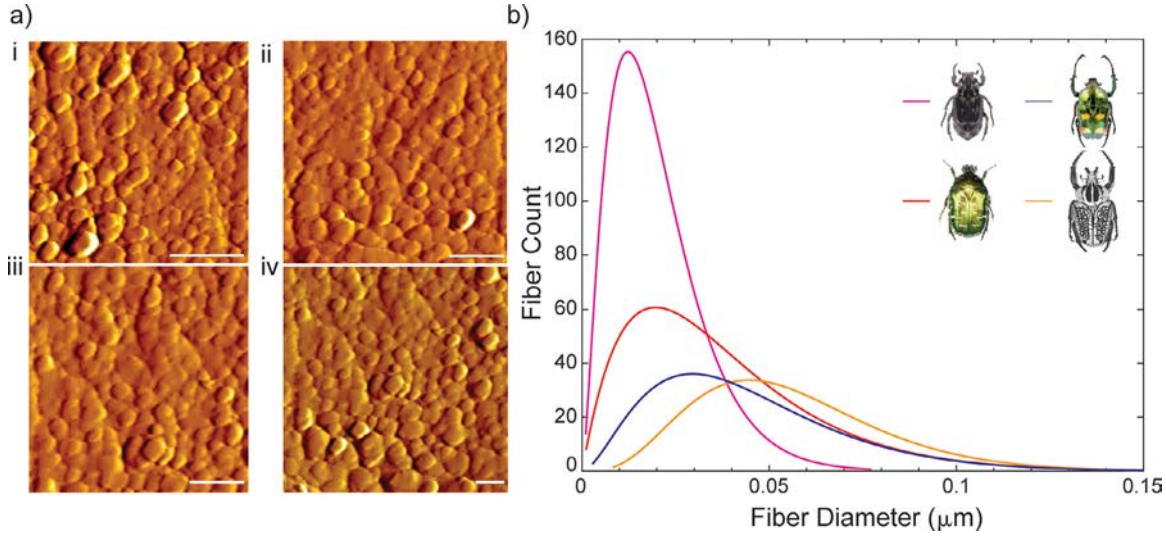

Fig. 4. Fiber diameter analysis. a) AFM images of selected exocuticle regions in Valgus hemipterus (i), Cetonia aurata pisana (ii), Jumnos ruckeri (iii) and Goliathus orientalis (iv). Scale bar: 50 nm b) Statistical distribution of fiber diameters for each species.

is not only consistent across the analyzed species but is also in concert with similar investigations performed in *Cotinis mutabilis*, also a member of the Cetoniinae subfamily [14].

Heterogeneity in the microstructure of biological materials has remarkable implications on the resistance of those materials to failure and fracture in response to mechanical loads. One of the main sources of such properties is the natural complex hierarchical arrangement of the constituents often coupled with functional gradients within the material, giving rise to hierarchical-functional gradients. The first evidence of such graded motifs is observed in the macroscopic thickness variation of the forewing (Figure S0), from the hinge to the pygidium, and the microscale

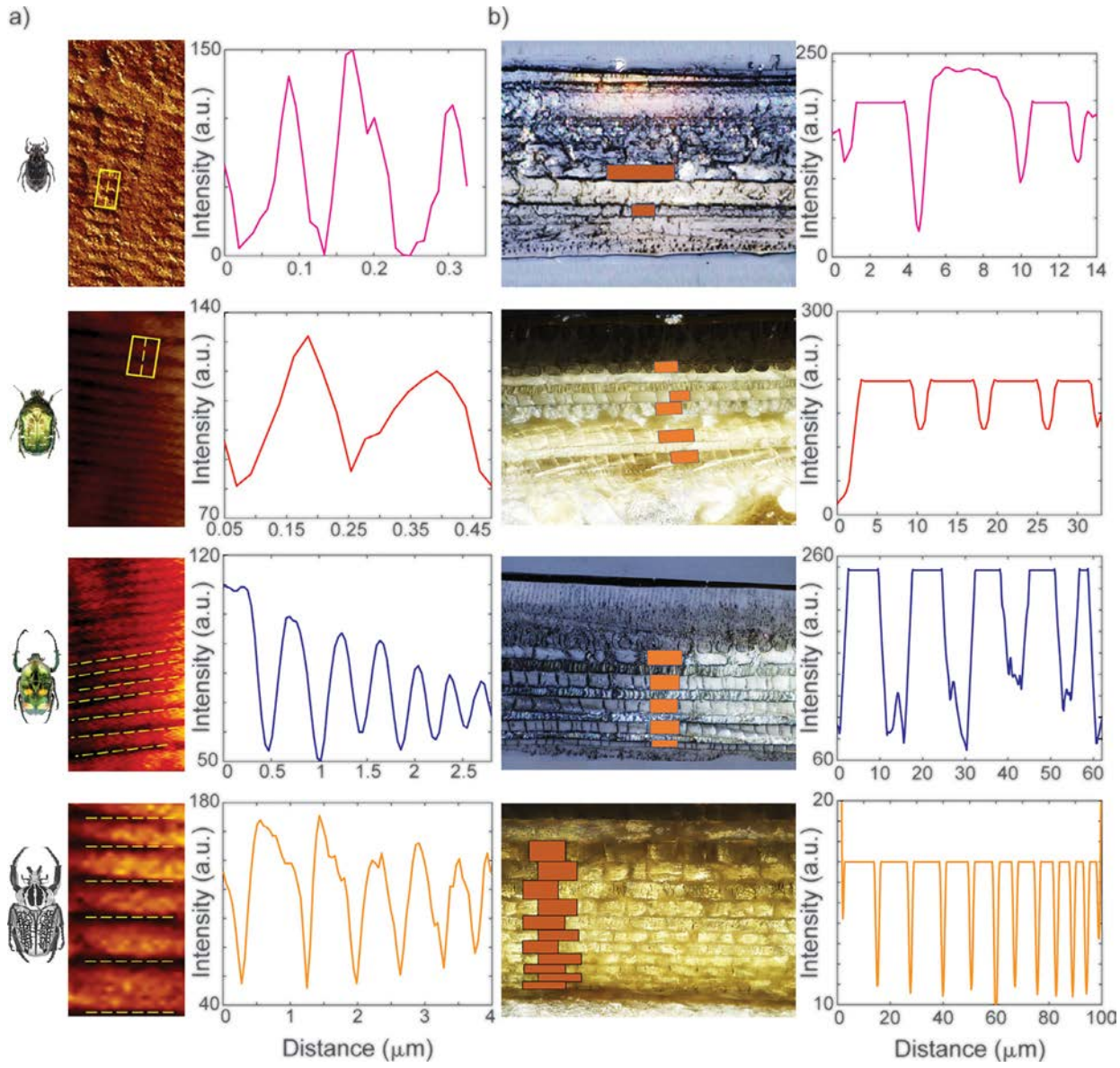

Fig. 5. AFM and Confocal microscopy images revealing size gradients in the (a) Exocuticle and (b) Endocuticle of *Valgus hemipterus, Cetonia aurata pisana, Jumnos ruckeri* and *Goliathus orientalis* (top to bottom).

thickness variation of the two most prominent elytral levels, the exo- and the endocuticle (Fig.2). At even smaller scales, both within the exo- and endocuticle, the presence of dimensional gradients is ubiquitous. Inside the exocuticle, the helicoidal motif, an orientation-graded structure in itself, displays a graded pattern, where the pitch length (p_{exo}) increases from the epicuticle-exocuticle interface towards the exocuticle-endocuticle interface. This pattern is consistently observed in the four selected beetles, each one differing in the rate of change between the pitch of adjacent units (Fig. 5a), with the commonality that the pitch size experiences less variation by increasing the distance from the interfacial layer between the exocuticle and the endocuticle. A focal point for the observation of functional gradients within biological materials is at the interfaces between their different substructures [17] where such natural gradients aid to smoothen the transition between the different properties of the two adjacent substructures. Similarly, in the endocuticle, the thickness of the layers in the pseudo-orthogonal plies presents a smooth decreasing variation from the exocuticle-endocuticle interface to the Hemolymph space (Fig. 4b).

3.3. Nanoscale properties of exocuticle fibers

AFM indentations on the fibers comprising the exocuticle of each beetle further point to similarities at the building block level of these natural composites (Fig. 6a). The indentation moduli along a single pitch in the exocuticles of the four beetles are presented in Fig. 6b, where the observed trend is consistent and analogous to the topographical trend observed in similar AFM measurements in scanning mode (Fig. 5). The ascending-descending trend observed, corresponding to points within the two symmetric half-pitches (i.e., 0°-90°, 90°-180°), is an indication of the anisotropic nature of the fibers. Along a given pitch, the indentation modulus attains its maximum and minimum values when indenting the transverse section and the lateral side of the fiber, respectively. Across species, only slight differences in indentation moduli are

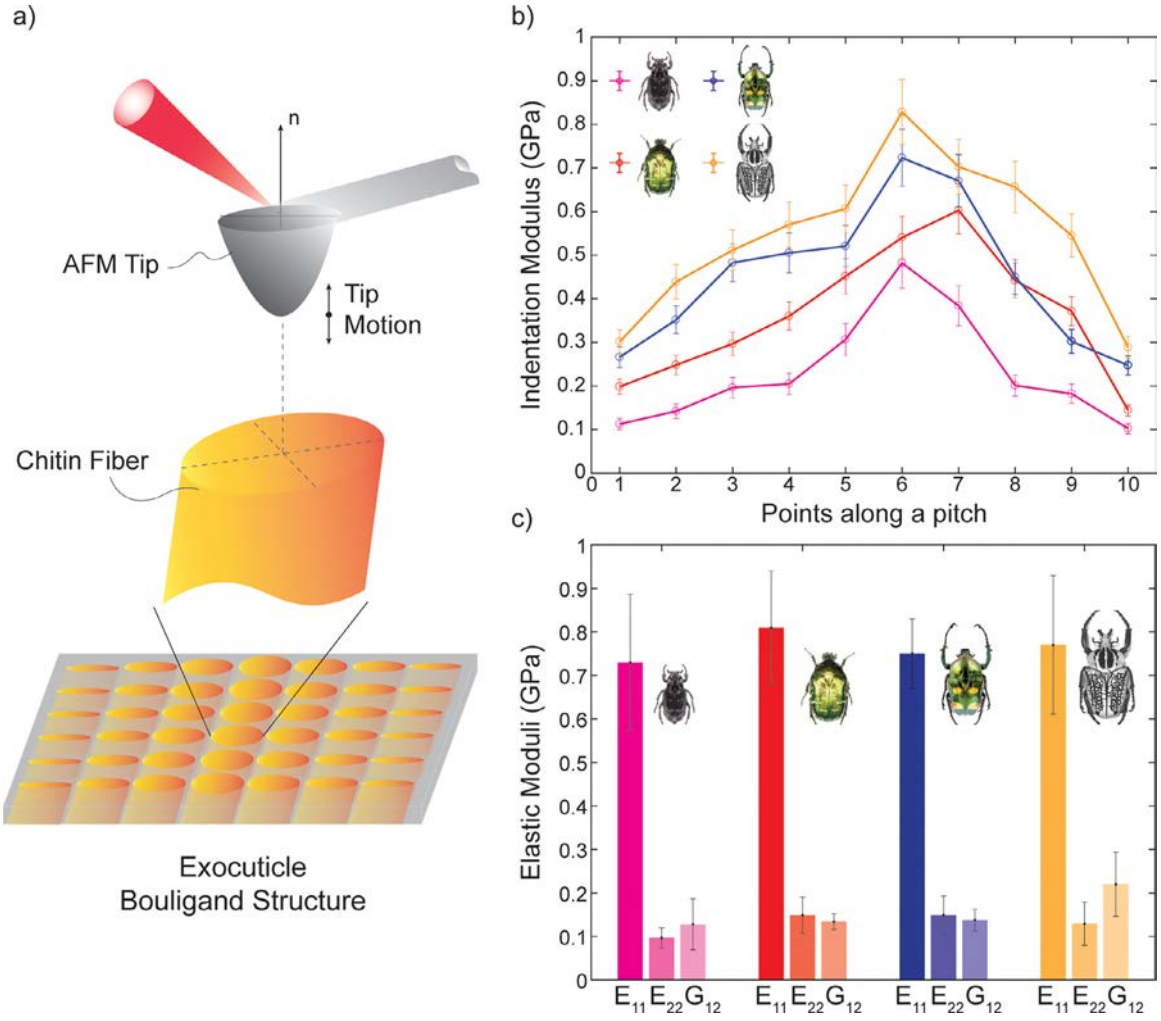

Fig. 6. Nanomechanical properties of exocuticle fibers. a) Schematic diagram of AFM indentation procedure to probe mechanical properties of the fibers. b) Variation of indentation modulus and c) Derived fiber elastic constants along an exocuticle pitch in Valgus hemipterus, Cetonia aurata pisana, Jumnos ruckeri and Goliathus orientalis.

observed (Fig. 6b). Despite differences in indentation moduli, calculation of elastic constants reveals similar values throughout the four beetle species, and presents good accord with the results previously obtained in *Cotinis mutabilis* (*Gory and Percheron*, 1883) [14, 18].

3.4. Compositional analysis

Energy dispersive spectroscopy (EDS) elemental maps of polished elytral cross sections and selected exocuticular and endocuticular regions reveal the distribution of the main chemical elements present in the elytra of the four studied beetles. Carbon (C), Oxygen (O) and Nitrogen (N) alone were consistently obtained, throughout the four species, without significant intraspecific and interspecific local variations (Fig. 7a-b, Figure S1) or gradients. Furthermore, presence of minerals or heavy metals was not found, notwithstanding the precedent of these components in sclerotized mandible cuticles in a number of insect orders, including Coleoptera [19]. The pervasive occurrence of Carbon, Oxygen and Nitrogen responds to the presence of chitin as building block of the elytra [20]. Chitin, the linear polymer of β-1,4-linked N-acetylglucosamine ($C_8H_{15}NO_6$), constitutes the lowest hierarchical level within the beetle's exocuticle, a feature shared though the Phylum *Arthropoda* but also with fungi, diatoms, and corals [21]. In beetles, particularly, chitin adopts a crystal form (primarily the α-chitin polyform) and bundles with cuticular proteins (CP) to form nanofibrils and aggregates of nanofibrils, which ultimately compose the helicoidal and pseudo-orthogonal arrangement observed in the exo- and endocuticle.

Fourier Transform Infrared Spectroscopy (FTIR) consistently revealed the presence of a number of functional groups along the elytra, again without evidencing significant spatial differences (Fig. 7c-d). The peaks found at λ*~2930 cm^{-1}* and λ*~3260 cm^{-1}* are associated to *C-H* stretching modes and the two peaks with similar intensities found at λ*~1650 cm^{-1}*, *1620 cm^{-1}* and λ*~1550 cm^{-1}* respond to the presence of Protein Amide I and Protein Amide II, respectively, characteristic of α-chitin and amino glycoproteins [22–24]. Bands at λ*~1250 cm^{-1}*, *1150 cm^{-1}*, λ*~1115 cm^{-1}*, *1072 cm^{-1}*, *1025cm^{-1}* and λ*~950 cm^{-1}* correspond to *C-N* stretching, *C-O* stretching, and *C-H* out of plane bending vibration modes, respectively [24,25]. Our findings on an elytra composition based on chitin and amino glycoprotein, without marked gradients, add to previous similar findings on beetles from the *Coccinellidae* [26], *Tenebrionidae* [27] and *Curculionidae* [20] subfamilies.

3.5. In situ SEM elytra mechanical testing

The bending performance of the elytra was studied *in situ* SEM to characterize the stiffness (in the small deformation regime) and the flexural strength, specific energy absorption, and failure mechanisms (in the large deformation regime up to failure), in the context of physiologically relevant loads.

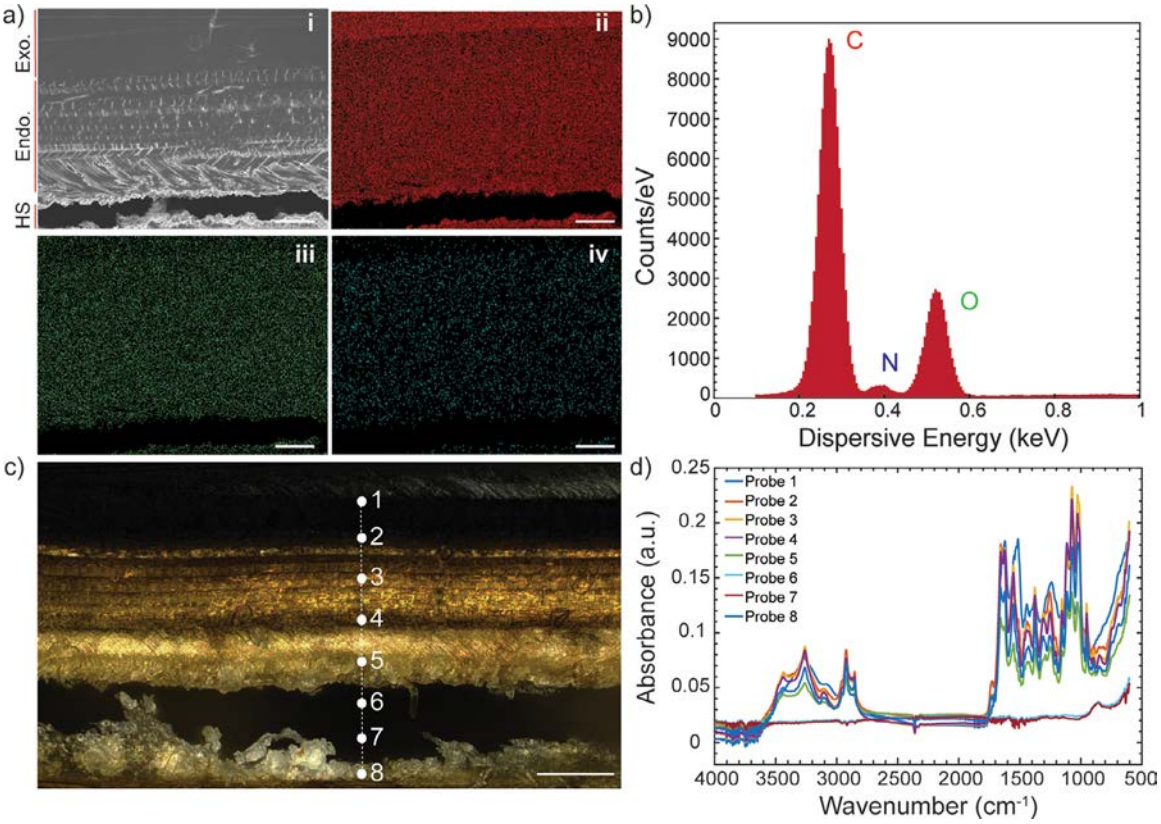

Fig. 7. Compositional analysis of beetle elytra. a) EDS element maps of the dorsal elytra of *Goliathus orientalis* (i), revealing widespread presence of Carbon (ii), Oxygen (iii) and Nitrogen (iv). Scale: 50 μm b) Dispersive energy peaks corresponding to EDS analysis. c) Probe points for FTIR analysis across the exocuticle of *Goliathus orientalis*. Scale: 100 μm. d) Absorption peaks from FTIR analysis of points in (c).

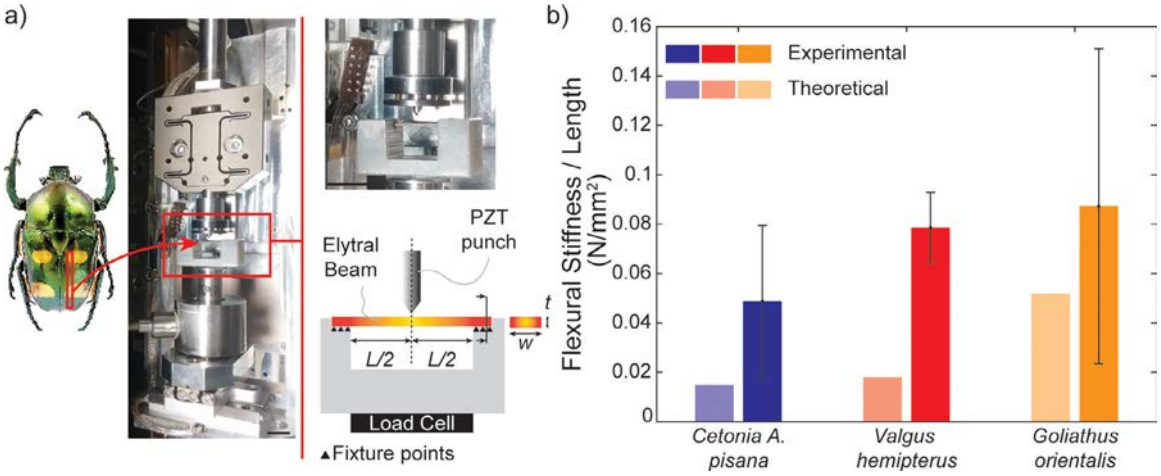

Fig. 8. Small deformation in situ SEM three-point bending test of beetle elytra. a) Actual experimental setup with nanomechanical platform and schematic setup with relevant dimensions, loads and fixtures. Scale: 10 mm. b) Experimental and theoretical estimates of the flexural stiffness, normalized by beam length, of Cetonia A. pisana, Valgus hemipterus and Goliathus orientalis elytral beams.

First, the bending response of beams, made of longitudinal sections from the central region of the elytra (Fig. 8a), was measured at small beam deflections. The bending stiffness was extracted from the slope of the initial linear segment of the loading curve (Fig. 8b, S2). Noteworthy, even at relatively small deflections, nonlinearities in the force-displacement signatures emerge and hysteretic loops upon unloading were observed. This is associated to the viscoelastic response of chitinous and proteinaceous building blocks in the elytra.

Second, to relate the identified layer architecture and measured fiber properties (see Section 3.2-3.4) to the mechanical performance of the elytra, we employed an analytical model to compute the beam equivalent flexural stiffness, normalized by beam length. The composite laminate theory (CLT) model is given in Appendix B: *Analytical Model for Elytral Beams*. A comparison between analytical predictions and experimental measurements (including standard deviations) is given in Fig. 8b. Given the elytra structural complexity and inherent variability in load-deflection signatures, as identified by this work and in Kundanati et al. [28], the agree-

ment and trends as a function of size, enables us to infer a very mild stiffness increase, as macroscopic size increases, despite three orders of magnitude in weight variation.

3.5.1. Failure mechanics and energy dissipation

A representative force-displacement curve obtained from bend testing, up to failure, in *Goliathus orientalis* is given in Fig. 9a. At test pauses, intermittent load drops are registered due to viscoelastic relaxation in the sample. The true mechanical response of *Cetonia aurata pisana, Jumnos ruckeri* and *Goliathus orientalis*, accounting for the viscous effect, are presented and compared in Fig. 9b. Finally, the maximum flexural stress, calculated from the maximum load and the expressions given in Appendix B, as well as the specific energy dissipation, area under the load-displacement curve normalized per unit sample mass (e), are depicted in Fig. 9c. As evident from Fig. 9c, and considering the inherent degree of variability, the peak flexural stresses and energy dissipation appear to be size independent, in spite of the size differences among beetles. Figs. 9d and Supplementary Figures S3-S7, illustrate the progression of deformation and a number of extrinsic toughening mechanisms (i.e., crack bridging, meandering and deflection, and arrest) and failure mechanisms (i.e., delamination, fiber pull-out, fiber breakage, buckling) occurring in tandem. Similarly, the failure progression and mechanical behavior of *Cetonia aurata pisana* and *Jumnos ruckeri* are detailed in Supplementary Figures S8-S12. The sequence of mechanisms, pervasively observed throughout the tested species, can be described as follows:

1 In concert with load increase, cracks first emerge within the endocuticle and propagate throughout the test following ply interfaces (i.e., interfaces constitute paths of minimum resistance). Concurrent shear deformation in the connecting trabecular elements, leads to coalescence of hemolymph space voids and subsequent separation of endocuticle plies (Fig. 9d, iii). Separation of these layers is evident by the stretching of fibers perpendicular to the beam length.
2 Stretching of the layers, below the neutral axis and in the vicinity of the punch, result in fiber breakage and fiber pull-out (Fig. 9d-iv). Upon further crack growth in the ventral cuticle, evidence of delamination is observed (Figure S3). As the beams bend, fibers within the lower layers are observed to separate from the matrix and pull-out allowing the crack to grow along the fibers. This observation is recognized as a key toughening mechanism whereby the dissipated energy is accumulated during fiber sliding, overcoming the fiber-matrix friction and pulling-out the fibers while propagating the crack through the matrix [29]. This mechanism is observed in all beetles (Figures S8, S13).
3 Shear forces between the ventral and dorsal cuticles lead to failure of the trabeculae, subsequent coalescence of hemolymph spaces and delamination within the endocuticle layer. While the lower layer of the beam, in the middle of the span and in proximity to the punch, experiences tensile stresses, the same layer experiences compressive stresses in the rgions of the supports. Indeed, buckling of the ventral layers near the supports is observed (Fig. 9d-v and Figures S4, S5). This mechanism is identified in all species (Figure S10, S12), and follows local failure of endocuticle sublayers.
4 In the small deformation regime, the top layer above the neutral axis is under compression. This is reversed as the load increases and deformations become large, which causes the emergence of small cracks in the epicuticle, near the supported regions. Following nucleation, these cracks propagate from the epicuticle to the exocuticle. Interestingly, the cracks are unable to further propagate into the endocuticle and are effectively arrested at the exocuticle-endocuticle interface (Inset Fig. 9d-v). Energy dissipation along the helicoidal microstructure of the exocuticle prevetns the crack from overcoming the energy barrier necessary to propagate through the endocuticle, which is revealed by the tortuosity of the crack edges and surface roughness of the fracture surfaces, consistent with measured exocuticle helicoidal pitches (Figure S7). Emergence of new cracks at the epicuticle further indicates the competition between nucleation and exo-to-endocuticle propagation. As the stress builds up, cracks are deflected and propagate along the exocuticle-endocuticle interface (i.e., crack channeling). The process is well captured in Figure S6. Notably, this failure sequence was only observed in *Goliathus orientalis*, suggesting a size dependence.
5 At the late stages of loading, cracks coalesce and propagate at the point of the contact between the punch and the beam (Figure S3), owing to stress concentration (i.e., local failure mode). Towards the end of the test, this local failure mode grows and, when combined with the delamination of the lower layers, leads to ultimate failure of the beam.

4. Discussion

The present work gravitates around two main facts: beetles constitute the most diverse order of insects and biological diversity is often a matter of size; and, as such, seeks to answer the question: *How does the structure-property-function relationship in a vital structure, as the elytra, respond to size variations in closely related beetles?* To such end, a number of multiscale characterizations were pursued to compare the elytra of four beetle species from the same subfamily but spanning three orders of magnitude in weight.

Unlike the ample body of literature devoted to particular aspects of beetle elytra of single species (e.g., stag beetles for their agonistic demeanor, dung beetles for their rolling capacity), this work differentiates itself by its integral comparative approach across species driven by the issue of scaling. To the authors' best knowledge, only the works on elytral microstructures of 40 beetles from 23 different families by Van de Kamp [10], and the mechanical studies by Yu and Xiang [31–34] compared beetles. Despite not addressing the issue of scaling, these studies recognized the scientific value of scaling due to the known influence of size at the individual (structure-function relationships) and social level (inter-/intraspecific interactions) [30]. In contrast to these broader studies, this work is focused on comparisons within a single subfamily driven by large variations in macroscopic size. The more focused nature of the study, reduces genetic variability, thus ensuring similar structures and functionality, while allowing sufficient size variability to capture scaling behavior.

The correlation of microstructural parameters, in the form of elytral thicknesses, with body masses in the form of power-law relationships, seems to point to the existence of evolutionary negative allometric laws underlying the biomechanical design of these structures in response to size variations. The fact that these structures and substructures do not scale isometrically are indicative of a complex interplay between the natural selection for size and efficiency, and the mechanical constraints which bound these structures. This finding makes beetle elytra one more exponent of biological scaling, a phenomenon that pervasively manifests itself in Nature [35]. The fact that the elytral thickness and exocuticle thickness present similar scaling exponents highlights the relevance of the exocuticle to the organism as the first mechanical barrier against puncture and piercing (as reflected via *in situ* SEM tests). Conversely, the lower exponent of the endocuticle could be related to the function of flight where endocuticle thickness is sacrificed for greater hemolymph space, thus resulting in lighter yet functionally stiff structures.

Allometric scaling laws, however, constitute only one aspect of the natural strategies to cope with a large operational size range.

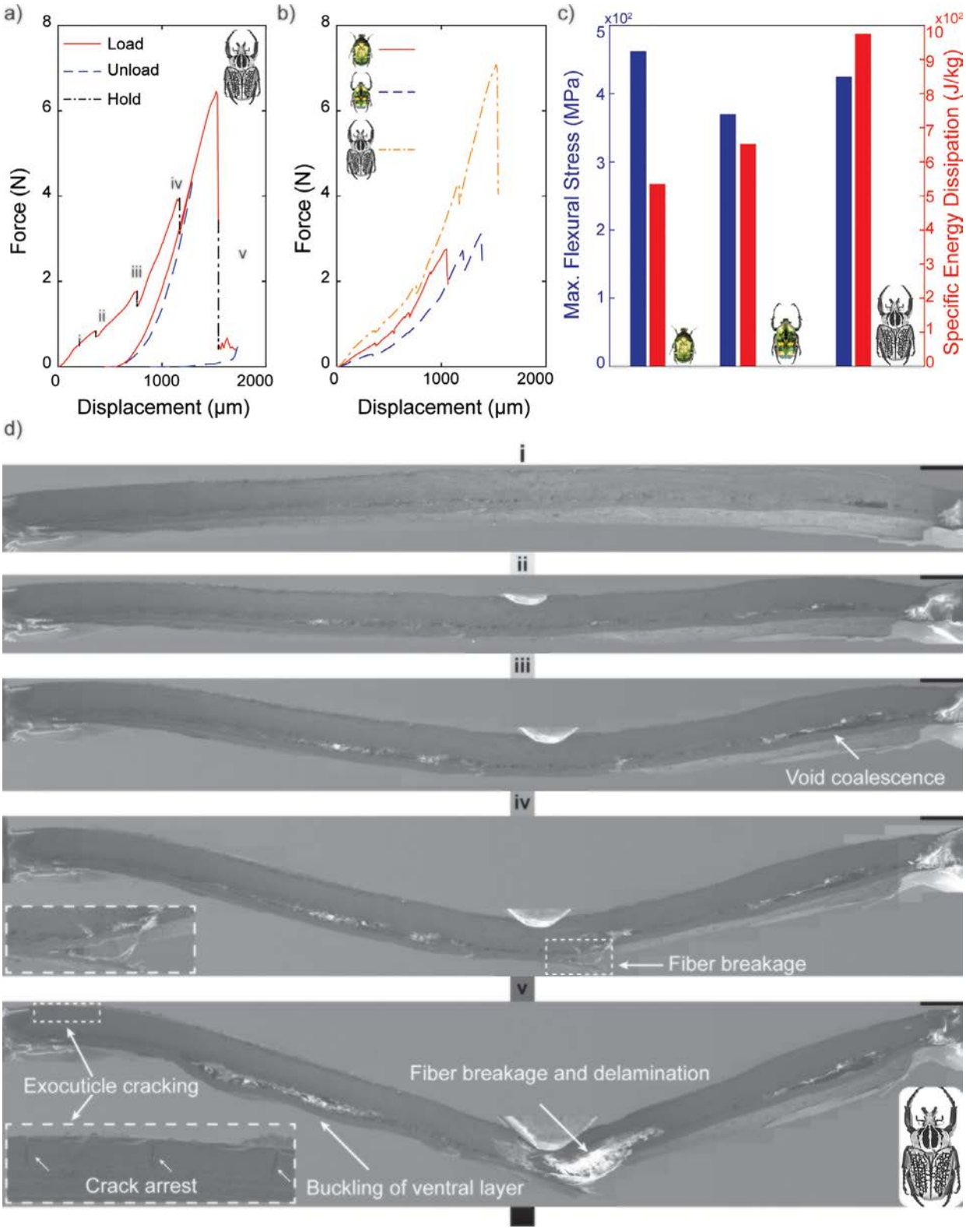

Fig. 9. In situ SEM three-point bending tests of beetle elytra upto failure. a) Force-displacement curves of Goliathus orientalis. b) Structural response of Cetonia aurata pisana, Jumnos ruckeri, and Goliathus orientalis. c) Maximum flexural stresses (left axis/bars) and specific energy dissipations (right axis/bars). d) SEM snapshots corresponding to roman numerals in a) and failure mechanisms in Goliathus orientalis. Scale bar: 400 μm.

The second aspect is comprised by a set of invariant features composed of foundational components (i.e., chemical and material building blocks) and design choices (i.e., material architectures, graded material-structural motifs), all of which have been found in the species studied. The identification of a similar chemistry, a similar layered layout, a helicoidal exocuticle and an endocuticle exhibiting an orthogonal fiber bundle morphology are not surprising, but were expected as conserved traits, imposed by developmental constraints (i.e., compositional, physical or dynamical limitations on phenotypic traits variation). As such, both the scaling laws and the conserved traits emphasize the concept of an adapted *bauplan* and contrast the interplay between developmental and evolutionary drivers. Also noteworthy is the first identification of dimensional gradients in the exo- and endocuticle of beetles, which coupled to similar observations in vertebrate and invertebrate taxons, points to the work of convergent evolution [36,37].

As revealed by *in situ* SEM bending tests, the combination of invariant (developmental) and scalable (allometric) features in the beetle elytra yield optimal structures in a symmorphosis sense (i.e., the regulation of biological units for an optimal outcome), fine-tuned to cope with mechanical pressures [35]. The integration of these similar and dissimilar features interestingly gives rise to similar mechanical performances in terms of stiffness, strength and energy absorption, facilitated by a multitude of shared toughening and failure mechanisms. In this respect, the use of simple mechanical models, integrating data from spatial and material multiscale characterizations also seem to point at the existence of similar mechanical performances, notwithstanding the overbearing differences in macroscopic size. These observations suggest that despite beetle size, mechanical functionality is conserved by ensuring similar levels of protection and the necessary bending and torsional stiffness to support flight. These results agree with the allometric invariances in mechanical design reported by Juang et al. in avian eggs [38], the extrinsic toughening mechanisms in *Macraspis lucida* [29] and the bending performance in *Lucanus cervus* [28], thus revealing traits that surpass taxonomy at the family level.

The present work undoubtedly opens a vista of opportunities for future work. Amongst these, investigations with a greater number of samples and sizes from the *Cetoniinae* subfamily are bound to provide additional information on the power-law relationships relating microstructural and mechanical performance to body weight. Though the allometric scaling found is expected to remain valid, the scaling exponents may be subject to improvement. In this regard, correspondence of such exponents to the commonly encountered quarter-power law (i.e., allometric exponents as simple multiples of 1/4) is intriguing [35]. The search for allometric scaling could also be extended within and across families. Extension of the present methodology to the latter promises to offer greater insight on the influence of selective pressures (i.e., survival vs. developmental constraints) on these biomaterials, still an unresolved issue. In this sense, the comparison of beetles facing radically different environments (e.g., water and terrestrial beetles) could represent an intriguing avenue of research. Further along this line, the incorporation of phylogenetic information into phylogenetically-informed regression models could shed further insight into the historical diversity and evolution of phenotypic traits [39,40]. Testing of elytral samples under beam bending has revealed a considerable degree of variability, as also detected by Kundanati et al. [28] who reported flexural moduli in *Lucanus cervus* of 811 ± 650 MPa. This stems from the inherent variability of biological composites, the heterogeneous and random nature in material distribution (e.g., voids in the hemolymph space), the small size of probed features (e.g., fiber diameter), and potential issues associated to sample preparation and handling. However, the use of analytical models with microstructural inputs can aid in elucidating comparative relationships, as shown here. The development of new mechanical testing protocols, the incorporation of multiscale approaches and a thorough characterization of the void distribution in the hemolymph space could potentially reduce variability. Lastly, the mechanical characterization of hydrated samples, more physiologically relevant, is left for future investigations due to the recognized effects of hydration on mechanical properties.

5. Conclusions

Elytra distinguishes beetles from all other insect orders and are widely acknowledged as a key biomechanical trait. Cross-species comparisons, particularly daunting for the Coleoptera order, and the study of mechanical properties of biological composites have traditionally pertained to the separate realms of biology and engineering, respectively, despite the ostensible links that bind mechanical performance to biological functionality. In an attempt to bridge the aforementioned fields, integral comparisons encompassing the macro-, micro- and nanostructure of four beetle species from the same taxonomical subfamily were undertaken to understand the adaptation of the elytra *bauplan* to changes in body size spanning three orders of magnitude. Our studies reveal the workings of a natural strategy combining both invariant and scalable features to synergistically accommodate size changes while maintaining functionality. On the one hand, the use of identical chemical and material building blocks together with layered-fibrous material architectures and dimensionally graded motifs were consistently observed in all species. On the other hand, negative allometric relationships and adjustments in fibrous building blocks seem to underlie the adjustment of elytral layers to body size. Despite the substantial differences in size, the integration of size-dependent and size-independent strategies manages to endow each beetle with similar specific mechanical performance (stiffness, strength, and energy absorption capabilities) together with an array of toughening mechanisms to ensure biomechanical functionality pertaining to protection and flight. Further studies encompassing more diverse populations, with an emphasis on phylogenetics, promise to elucidate additional biological design rules that could be leveraged in the design of scalable synthetic composites.

Declaration of Competing Interest

The authors declare that they have no known competing financial interests or personal relationships that could have appeared to influence the work reported in this paper.

Acknowledgments

The authors gratefully acknowledge financial support from a Multi-University Research Initiative through the Air Force Office of Scientific Research (AFOSR-FA9550-15-1-0009). M.A. acknowledges support under the Postdoctoral Fellowships Program (NSERC PDF #516501-2018) from the Natural Sciences and Engineering Research Council of Canada. N.A.A. and H.D.E. gratefully acknowledge financial support from the Roberto Rocca Education Program (RREP). R.B. was supported by the National Science Foundation under NSF Award Number EEC-1757618. This work made use of the MatCI Facility at Northwestern University that receives support from the MRSEC Program (NSF DMR-1720139). Authors thank A. Zaheri, C. Shute, R. Bleher, M. Seniw, and T. Abbott for helpful discussions.

Supplementary materials

Supplementary material associated with this article can be found, in the online version, at doi:10.1016/j.actbio.2020.12.039.

References

[1] D. Maddison, Coleoptera beetles. http://tolweb.org/Coleoptera/8221/2000.09.11, 2000.
[2] J.Y. Sun, B. Bhushan, Structure and mechanical properties of beetle wings: a review, Rsc. Adv. 2 (33) (2012) 12606–12623.
[3] T.G. Barraclough, M.V.L. Barclay, A.P. Vogler, Species richness: does flower power explain beetle-mania? Curr. Biol. 8 (23) (1998) R843–R845.
[4] B.D. Farrell, Inordinate fondness" explained: why are there so many beetles? Science 281 (5376) (1998) 555–559.
[5] D. Grimaldi, M.S. Engel, M.S. Engel, T. Gale, Evolution of the Insects, Cambridge University Press2005.
[6] D.M. Linz, A.W. Hu, M.I. Sitvarin, Y. Tomoyasu, Functional value of elytra under various stresses in the red flour beetle, Tribolium Castaneum, Sci. Rep.-Uk 6 (2016).
[7] A.R. Parker, C.R. Lawrence, Water capture by a desert beetle, Nature 414 (6859) (2001) 33–34.
[8] T.Q. Le, T.V. Truong, S.H. Park, T.Q. Truong, J.H. Ko, H.C. Park, D. Byun, Improvement of the aerodynamic performance by wing flexibility and elytra - hind wing interaction of a beetle during forward flight, J. R. Soc. Interface 10 (85) (2013).
[9] A.E. Seago, P. Brady, J.P. Vigneron, T.D. Schultz, Gold bugs and beyond: a review of iridescence and structural colour mechanisms in beetles (Coleoptera), J. R. Soc., Interface 6 (2009) S165–S184.
[10] T. van de Kamp, A. Riedel, H. Greven, Micromorphology of the elytral cuticle of beetles, with an emphasis on weevils (Coleoptera: Curculionoidea), Arthropod. Struct. Dev. 45 (1) (2016) 14–22.
[11] A.C. Neville, Biology of Fibrous Composites: Development Beyond the Cell Membrane, Cambridge University Press, New York, NY, USA, 1993.
[12] J.L. Hutter, J. Bechhoefer, Calibration of atomic-force microscope tips, Rev. Sci. Instrum. 64 (7) (1993) 1868–1873.
[13] D.A. Walters, J.P. Cleveland, N.H. Thomson, P.K. Hansma, M.A. Wendman, G. Gurley, V. Elings, Short cantilevers for atomic force microscopy, Rev. Sci. Instrum. 67 (10) (1996) 3583–3590.
[14] R.G. Yang, A. Zaheri, W. Gao, C. Hayashi, H.D. Espinosa, AFM identification of beetle exocuticle: bouligand structure and nanofiber anisotropic elastic properties, Adv. Funct. Mater. 27 (6) (2017).
[15] R. White, Beetles, Houghton Mifflin Harcourt, 1998.
[16] A.J. Spence, Scaling in biology, Curr. Biol. 19 (2) (2009) R57–R61.
[17] Z. Liu, M.A. Meyers, Z. Zhang, R.O. Ritchie, Functional gradients and heterogeneities in biological materials: design principles, functions, and bioinspired applications, Prog. Mater. Sci. 88 (2017) 467–498.
[18] J.J. Vlassak, M. Ciavarella, J.R. Barber, X. Wang, The indentation modulus of elastically anisotropic materials for indenters of arbitrary shape, J. Mech. Phys. Solids 51 (9) (2003) 1701–1721.
[19] D.L.J. Quicke, P. Wyeth, J.D. Fawke, H.H. Basibuyuk, J.F.V. Vincent, Manganese and zinc in the ovipositors and mandibles of hymenopterous insects, Zool. J. Linn Soc.-Lond. 124 (4) (1998) 387–396.
[20] X. Wu, A. Erbe, D. Raabe, H.O. Fabritius, Extreme optical properties tuned through phase substitution in a structurally optimized biological photonic polycrystal, Adv. Funct. Mater. 23 (29) (2013) 3615–3620.
[21] N.S. Gupta, Chitin: Formation and Diagenesis, Springer, Dordrecht; New York, 2011.
[22] M. Kaya, E. Lelesius, R. Nagrockaite, I. Sargin, G. Arslan, A. Mol, T. Baran, E. Can, B. Bitim, Differentiations of chitin content and surface morphologies of chitins extracted from male and female grasshopper species, PLoS One 10 (1) (2015).
[23] A.T. Paulino, J.I. Simionato, J.C. Garcia, J. Nozaki, Characterization of chitosan and chitin produced from silkworm crysalides, Carbohyd. Polym. 64 (1) (2006) 98–103.
[24] H. Ehrlich, M. Maldonado, K.D. Spindler, C. Eckert, T. Hanke, R. Born, C. Goebel, P. Simon, S. Heinemann, H. Worch, First evidence of chitin as a component of the skeletal fibers of marine sponges. Part I. verongidae (Demospongia: porifera), J. Exp. Zool. 308b (4) (2007) 347–356 Part B.
[25] R.A. Nyquist, Interpreting Infrared, Raman, and Nuclear Magnetic Resonance Spectra, Academic Press, San Diego, 2001.
[26] J.W. Xiang, J.X. Du, D.C. Li, C. Zhen, Functional morphology and structural characteristics of wings of the ladybird beetle, Coccinella septempunctata (L.), Microsc. Res. Techn. 79 (6) (2016) 550–556.
[27] N.M.H. Zohry, A.M. El-Sayed, Morphology, histology, and chemistry of the wings of Tribolium castaneum and Tribolium confusum (Coleoptera: Tenebrionidae), J. Basic Appl. Zool. 80 (1) (2019) 16.
[28] L. Kundanati, S. Signetti, H.S. Gupta, M. Menegon, N.M. Pugno, Multilayer stag beetle elytra perform better under external loading via non-symmetric bending properties, J. R. Soc. Interface 15 (144) (2018).
[29] D. Sykes, R. Hartwell, R.S. Bradley, T.L. Burnett, B. Hornberger, R.J. Garwood, P.J. Withers, Time-lapse three-dimensional imaging of crack propagation in beetle cuticle, Acta Biomater. 86 (2019) 109–116.
[30] G.A. Bartholomew, A matter of size: an examination of endothermy in insects and terrestrial verterbrates, in: B. Heinrich (Ed.), Insect thermoregulation, Wiley, New York, 1981.
[31] J.X. Chen, J. Xie, Z.S. Wu, E.M.A. Elbashiry, Y. Lu, Review of beetle forewing structures and their biomimetic applications in China: (I) On the structural colors and the vertical and horizontal cross-sectional structures, Mater. Sci. Eng., C 55 (2015) 605–619.
[32] C. Xiang, Mechanism of Natural Composite Materials and Composite Materials Research Coleoptera Insects Bionic Design—It's Gradual Microstructure and Mechanical Behavior, Chongqing University, 1994.
[33] C. Xiang, J. Fan, On the strengthening and toughening mechanism of natural composites and research of biomimetic composites, Adv. Mech. 24 (2) (1994) 232 220.
[34] M. Yu, I. Hermann, Z.D. Dai, N. Gitis, Mechanical and frictional properties of the elytra of five species of beetles, J. Bionic Eng. 10 (1) (2013) 77–83.
[35] J.H. Brown, G.B. West, B. Enquist, Scaling in biology: patterns and processes, causes and consequences, in: J.H. Brown, G.B. West (Eds.), Scaling in Biology, Oxford University Press, New York, 2000.
[36] D. Raabe, C. Sachs, P. Romano, The crustacean exoskeleton as an example of a structurally and mechanically graded biological nanocomposite material, Acta. Mater. 53 (15) (2005) 4281–4292.
[37] J.C. Weaver, G.W. Milliron, A. Miserez, K. Evans-Lutterodt, S. Herrera, I. Gallana, W.J. Mershon, B. Swanson, P. Zavattieri, E. DiMasi, D. Kisailus, The stomatopod dactyl club: a formidable damage-tolerant biological hammer, Science 336 (6086) (2012) 1275–1280.
[38] J.Y. Juang, P.Y. Chen, D.C. Yang, S.P. Wu, A. Yen, H.I. Hsieh, The avian egg exhibits general allometric invariances in mechanical design, Sci. Rep. 7 (2017).
[39] P.H. Harvey, Why and how phylogenetic relationships should be incorporated into studies of scaling, in: J.H. Brown, G.B. West (Eds.), Scaling in Biology, Oxford University Press, New York, 2000.
[40] L.Z. Garamszegi, Modern Phylogenetic Comparative Methods and Their Application in Evolutionary Biology: Concepts and Practice, Springer, Berlin, 2014.